An AZA-Fused π-Conjugated Microporous Framework Excellent Catalyst for the Production of Hydrogen Peroxide

V. Briega-Martos,[†] A. Ferre-Vilaplana,[‡,§] A. de la Peña,[⊥,Σ] J. L. Segura,[⊥] F. Zamora,*[,Σ] J. M. Feliu,[†] and E. Herrero*[,†]

[†] *Instituto de Electroquímica, Universidad de Alicante, Apdo 99 E-03080, Alicante, Spain*

[‡] *Instituto Tecnológico de Informática, Ciudad Politécnica de la Innovación, Camino de Vera s/n, E-46022 Valencia, Spain*

[§] *Departamento de Sistemas Informáticos y Computación, Escuela Politécnica Superior de Alcoy, Universidad Politécnica de Valencia, Plaza Ferrándiz y Carbonell s/n, E-03801 Alcoy, Spain*

[⊥] *Departamento de Química Orgánica, Facultad de Química, Universidad Complutense de Madrid, E-28040, Madrid, Spain*

[Σ] *Departamento de Química Inorgánica e Instituto de Física de la Materia Condensada (IFIMAC), Facultad de Ciencias. Universidad Autónoma de Madrid, E-28049, Madrid, Spain*

ABSTRACT: The electrochemical production of hydrogen peroxide can be implemented in small-scale plants under "on demand" approach. For that, selective catalysts for the oxygen reduction reaction (ORR) towards the desired species are required. Here, we report about the synthesis, characterization, ORR electrochemical behavior and reaction mechanism of an aza-fused π-conjugated microporous polymer, which presents high selectivity towards hydrogen peroxide. It was synthesized by polycondensation of 1,2,4,5-benzenetetramine tetrahydrochloride and triquinoyl octahydrate. A cobalt-modified version of the material was also prepared by a simple post-synthesis treatment with a Co(II) salt. The characterization of the material is consistent with the formation of a conductive robust porous covalent laminar poly-aza structure. The ORR properties of these catalysts were investigated using rotating disk and rotating disk-ring arrangements. The results indicate that hydrogen peroxide is almost exclusively produced at very low overpotential values on these materials. Density functional theory calculations provide key elements to understand the reaction mechanism. It is found that, at the relevant potential for the reaction, half of the nitrogen atoms of the material would be hydrogenated. This hydrogenation process would destabilize some carbon atoms in the lattice and provides segregated charge. On the destabilized carbon atoms, molecular oxygen would be chemisorbed with the aid of charge transferred from the hydrogenated nitrogen atoms and solvation effects. Due to the low destabilization of the carbon sites, the resulting molecular oxygen chemisorbed state, which has the characteristics of a superoxide species, would be only slightly stable and would promote the formation of hydrogen peroxide.

INTRODUCTION

Hydrogen peroxide is a commodity chemical used mainly as a bleaching agent, though it has other important applications, such as water disinfection. It is currently primarily produced using anthraquinone route. This is a complex process, which gives rise to side reactions, originating a net consumption of anthraquinone, and which requires of several separations. As a result, it can be only deployed effectively in large-scale plants. Moreover, the centralized production approach introduces additional drawbacks, such as large inversions, massive storage re-

quirements and costs of transport to the consumption sites. Therefore, an alternative and efficient production method, which can be implemented in small-scale plants to allow a distributed production on demand, would be a more convenient technology.

Interestingly, hydrogen peroxide is usually yielded as an undesired by-product of the oxygen reduction reaction (ORR) in fuel cells. In the complete ORR to water four electrons are exchanged. However, when only two electrons can be exchanged, hydrogen peroxide is produced. On the most part of catalysts, the ORR evolves simulta-

neously through both routes at different rates. For fuel cell applications, the catalyst must be optimized towards the complete reduction to water. However, ORR catalysts can be alternatively optimized towards the exchange of two electrons process, giving rise to the concept of electrochemical cell of production of hydrogen peroxide. The electrochemical synthesis of hydrogen peroxide could be implemented at the consumption site in small plant, adapting the production to the demand and avoiding the drawbacks inherent to a centralized production. Additionally, if the overpotential for the ORR was low, energy can be obtained from a cell where the anode reaction would be the hydrogen oxidation reaction, since the cell potential would be positive. Thus, finding appropriate catalysts with a low overpotential for the ORR producing exclusively hydrogen peroxide is very attractive for practical purposes. The cell can have the typical configuration of a polymer membrane fuel cell, in which hydrogen in which hydrogen peroxide is synthesized instead of water. Some years ago, only cationic (*aka*. acidic) membranes were available in the market, which restrict the use of this technology to electrocatalysts working in acidic media. However, the advent of reliable alkaline (anionic) membranes opens new possibilities for the use of electrocatalysts working in alkaline media.

Gold and doped platinum electrodes have shown good ORR activity for hydrogen peroxide production at low overpotentials.[1-4] However, the high cost of these metals prevents their use. On the other hand, under alkaline conditions, carbon materials are active for hydrogen peroxide production at relatively high overpotentials. When these materials are doped with nitrogen, their ORR activity improves, but increasing their selectivity towards the formation of water.[5-17] Computational results suggest that the ORR activity of these materials depends on the specific location of the nitrogen-dopants,[18-19] In a pair of previous works,[20-21] the role played by different forms of nitrogen-dopants in the activation of the molecular oxygen on graphitic materials has been elucidated. The need of destabilized carbons and available charge, and the role played by the hydrogenation of pyridinic nitrogen-dopants and the solvation effect was established. In view of those results, it can be argued that, for optimal hydrogen peroxide production purposes, a chemisorbed state of molecular oxygen, with superoxide characteristics and a small stability would be the ideal situation. A slightly adsorbed superoxide implicates a slightly adsorbed hydrogen peroxide anion, which favor their desorption, yielding hydrogen peroxide in the solution. Our previous results suggest that such a kind of active sites could be enabled by pyridinic nitrogen-dopants at the zigzag edges of graphitic materials.[21]

The assembling of porous materials from molecular building blocks allows the control not only of the composition but also of the microstructure and is essential for a heterogeneous catalyst. Aza-fused π-conjugated microporous polymers (Aza-CMP), which are assembled from molecular building blocks, present a high number of pyridinic nitrogen-dopants at edges with a zig-zag charac-

teristic. Additionally, they present a very well defined structure, with only one type of nitrogen functionality, which allows the identification of the active site and the mechanism using experimental and computational methods. These were studied by Kou *et al.* and they showed excellent electrochemical properties like large capacitance and high energy and power densities.[22] For these reasons, they have been selected as promising selective ORR catalysts towards hydrogen peroxide in this research. Here, we report about the synthesis, characterization, ORR electrochemical behavior and reaction mechanism of the aza-fused π-conjugated microporous polymer (**Aza-CMP**) shown in Figure 1, obtained by the polycondensation reaction with water formation between 1,2,4,5-benzenetetramine tetrahydrochloride and triquinoyl octahydrate. We have also studied the electrochemical behavior of the **Aza-CMP** modified with Co(II) because the incorporation of metals can lead to a modified activity.[14, 16] As will be shown, these materials exhibit high activity for hydrogen peroxide production at low overpotentials. Density functional theory (DFT) calculations provide insights in order to understand the reaction mechanism.

EXPERIMENTAL AND COMPUTATIONAL METHODS

Preparation of the Aza-CMP. 532.5 mg (1.875 mmol) of 1,2,4,5-benzenetetramine tetrahydrochloride in 15 mL of anhydrous DMF and 390 mg (1.25 mmol) of triquinoyl octahydrate in 5 mL of anhydrous DMF were mixed and refluxed for 48 h under argon. The dark brawn solid was purified upon hot extraction with methanol for 24 h using a Soxhlet. The resulting solid was dried under vacuum at 150 ºC for 24 h. Yield 304.6 mg (91 %). Elementary analysis for **Aza-CMP**, C (52.47 %), H (3.84 %), N (23.92 %). TGA indicates a mass loss of *ca.* 7 % between 20-250 ºC that is assigned to the solvent trapped at the pores. At 250 ºC the material starts its chemical decomposition.

Preparation of the Aza-CMP@Co. The **Aza-CMP** material was modified with Co(II) using two different reagents: cobalt(II) sulfate heptahydrate and cobalt(II) acetylacetonate (Co(acac)$_2$). In the first case, 25 mg of **Aza-CMP** were immersed in 3.7 mL of a 25 mg/mL CoSO$_4$·7H$_2$O in methanol solution. The suspension was stirred during 24 h at room temperature. The solid was filtered and then it was washed with methanol until the filtrate became colorless. Finally, the product was dried at 100 °C at vacuum conditions. With these quantities the Co:N molar ratio is 2:1, while after all the process this ratio in the obtained material is 1:293 (0.13 % wt. of Co). In the second case, 25 mg of **Aza-CMP** were immersed in 10 mL of a 2.8 mg/mL Co(acac)$_2$ in methanol solution. The subsequent procedure is the same as used for the CoSO$_4$·7H$_2$O. With these quantities the Co:N molar ratio is 2:3, and after all the process this ratio in the final material is 1:192 (0.20 % wt. of Co). Both modification procedures lead to very similar electrochemical behavior slightly better for the material prepared with CoSO$_4$·7H$_2$O. For

that reason, only the results of the Aza-CMP modified with cobalt sulfate are shown.

Preparation of the catalyst inks and the catalyst film on the electrode. For the preparation of the catalyst film on the electrode, the catalyst was first dispersed in a water/alcohol/Nafion ionomer solution to form an ink. The Nafion ionomer is added to enhance the adhesion of the catalyst film to the electrode surface.[23] The inks for all cases were prepared immersing 5 mg of the catalyst in a solution containing 4 mL of water, 1 mL of isopropanol (Merck, for analysis EMSURE®) and 50 µL of 5 wt% Nafion ionomer solution (Sigma-Aldrich). The catalyst ink was then transferred to an ultrasonicator and sonicated for 60 min. Before each measurement, the catalyst ink was sonicated to assure that the catalyst particles were well dispersed. Then, 10 µl of the ink were deposited onto the electrode fully covering the glassy carbon but avoiding the deposition on the Teflon shield. For drying the ink droplet, the electrode was rotated at 700 rpm and was kept in Ar atmosphere until the film was completely dry. By using this method, a reproducible and uniform film covering the entire glassy carbon surface was obtained.[23-24]

Electrochemical measurements. Two different experimental set-ups were used for the electrochemical measurements. First, the characterization of the electrodes and the ORR studies were performed using a glassy carbon rotating disk electrode (RDE), and the **Aza-CMP** and **Aza-CMP@Co** catalysts were deposited on this electrode. After these experiments, the quantification of hydrogen peroxide produced during the ORR was performed using a rotating ring-disk electrode (RRDE), composed of a glassy carbon disk (in which the catalyst film can be deposited) and a platinum ring where the hydrogen peroxide is detected. For both set-ups, the experiments were carried out at room temperature in a three electrode electrochemical cell de-oxygenated using Ar (Air Liquide, N50) for the electrode characterization. A gold wire was used as counter electrode and the reference electrode was a reversible hydrogen electrode (RHE) connected to the cell through a Luggin capillary. The working solutions were prepared using NaOH·H$_2$O (Merck, Suprapur 99.99%). Ultrapure water (Elga PureLab Ultra, 18.2 MΩ cm) was used for the preparation of the solutions and glassware cleaning.

For the ORR studies, the electrochemical cell was bubbled with O$_2$ (Air Liquide Alphagaz) until the solution was saturated. The experiments using a RDE were performed with an EDI101 rotating electrode and the rotation rate was controlled by a Radiometer CTV 101 apparatus. In this case, a signal generator EG&G PARC 175 and an eDAQ EA161 potentiostat with an eDAQ e-corder ED401 recording system were used for the electrochemical measurements. The RRDE experiments were carried out using a Pine AFMSRXE Electrode Rotator, and the electrochemical measurements were taken with an EG&G Bi-Potentiostat Model 366A and an eDAQ e-corder ED401.

In all cases, the glassy carbon electrodes were first polished with alumina from higher to lower particle sizes.

After this process, they were sonicated and finally rinsed with ultrapure water. Then, the electrodes were transferred to the electrochemical cell where a cleaning electrochemical procedure was performed: the electrode was cycled between 0.06 V and 1.7 V (*vs* RHE) until a stable cyclic voltammogram was obtained. For the RRDE measurements, the platinum ring was also cycled between 0.06 V and 1.7 V (*vs* RHE). After the electrode characterization and the ORR study on the bare electrode, the catalyst film was deposited for the electrochemical characterization and the study of its electrocatalytic activity. In the case of the RRDE, special care was taken to ensure that the ink droplet does not cover the platinum ring. For hydrogen peroxide detection at the platinum ring of the RRDE, the potential of the ring is maintained at 1.1 V (*vs* RHE) while the potential at the disk is swept between 0.06 V and 1.0 V (*vs* RHE). In the present cell conditions, the only species present in the cell solution that can be oxidized at 1.1 V is hydrogen peroxide (actually, for this pH value, HOO$^-$). Thus, the measured ring current is directly proportional to the amount of hydrogen peroxide formed on the disk.

Computational methods. The monodentate chemisorption of molecular oxygen on different sites of the investigated material was explored running different periodic DFT calculations under the GGA approximation and using the PBE functional[25] and numerical basis sets of double-numerical plus polarization quality[26] as implemented in the Dmol3 code.[27] Neutral and charged charge conditions compensated by a charge helium were considered. All the electrons were explicitly included in the calculations under a spin unrestricted approach. The effects of non-zero dipole moments in the cells were cancelled by means of external fields.[28] Full and partial optimizations were carried out depending on the goal.

Moreover, since previous results[20] indicate that solvation effects are important in the mechanisms, continuum solvation effects were taken into account by means of the COSMO model,[29] meanwhile hydrogen bonds were captured by including additional explicit water molecules as solvation effect treatment.[20] To verify the quality of the selected solvation effect treatment, solvation energies were computed for oxygen and superoxide, obtaining values that were found to be consistent with those expected.

The investigated material was modeled using a periodic cell comprising 42 graphitic atoms (30 carbon and 12 nitrogen atoms) and a vacuum slab of 20 Å. The shortest distance between periodic images was *ca.* 16.57 Å. Moreover, since previous results indicate that the hydrogenation of pyridinic nitrogen in graphitic materials could play a role in the molecular oxygen activation,[21] different hydrogenation states were explored searching for the relevant one.

An orbital cutoff radius of 3.7 Å was used in the numerical basis set for all the atoms. The optimization convergence thresholds were set to 1.0×10^{-5} Ha for the energy, 0.002 Ha/Å for the force, and 5.0×10^{-3} Å for the displacement. The SCF convergence criterion was set to 1.0×10^{-6} Ha for the energy. Brillouin zones were sampled, under

the Monkhorst-Pack method,[30] using grids corresponding to distances in the reciprocal space of the order of 0.02 1/Å, which was enough to avoid using thermal smearing as convergence aid. A value of 78.54 was used as the dielectric constant in the continuous solvation model.

In order to capture hydrogen bonds, for models targeted to visualization (Figure 8), an explicit water molecule was included in de model, in addition to the continuum solvation model, as solvation effect treatment. However, considering our previous results,[20] for models targeted to energetics evaluations (Figure 9) five explicit water molecules were included in the model, in addition to the continuum solvation model, as solvation effect treatment. A typical configuration of the formed explicit water solvation shell can be observed in the supporting information.

Chemisorbed states were searched for running full optimizations. The relevance of each one of them was established determining its stability. For such a purpose, the energetics for the shortest distances of the reactions paths were estimated performing several constrained optimizations. For each reaction path, the basic configuration and treatment was maintained, but the distance between the carbon acting as active site and the nearest atom of the oxygen molecule was varied and constrained during the optimization process. To facilitate comparisons, the displayed total energies were referred to their respective references, calculated as the adsorbent energy plus that corresponding to the adsorbate complex in the bulk. Note that only relatively short C-O distances were considered. Thus, the final convergence to the alignment level of the respective references, at very long distances, is not displayed. The reasons for doing so were three. First, it has been pointed out that, because of the required change in the spin multiplicity, non-adiabatic effects could be implicated in the chemisorption of a solvated oxygen molecule. Second, for some of the considered cases, long distances between adsorbent and adsorbate give rise to very challenging models for which states of different spin multiplicity are very close in energy. Third, when solvation effects are sufficiently captured, the available charge of the surface is assigned to the solvated oxygen molecule during the optimization process, giving rise to a solvated superoxide anion, even when the oxygen molecule has not even yet come close to the surface. All these difficulties are circumvented by considering only relatively short C-O distances. For the shortest distances, the required spin multiplicity change has already taken place, the most favorable spin multiplicity of the solutions are much more clearly defined, and an eventual charge transfer to oxygen can be better explained. All the calculations were run under automatic spin multiplicity conditions. For the relevant configurations, it was verified that, along the considered distances, the most favorable spin multiplicity was invariant. Despite of only the shortest distances were considered, still useful insights were derived about the investigated mechanism.

RESULTS AND DISCUSSION

Synthesis and characterization of the Aza-CMP material. Preparation of **Aza-CMP** was carried out following a different route to that previously used by Kou *et al.*[22] Indeed our approach does not use catalyst and solvothermal conditions but just a reflux of DMF (Figure 1). Thus, this preparation avoids contamination of the resulting material with the metallic catalyst, which can affect the electrocatalytic results.

The formation of **Aza-CMP** was confirmed by solid-state ^{13}C cross polarization/magic angle spinning nuclear magnetic resonance (CP-MAS NMR) (Figure S1) and FTIR spectroscopies (Figure S2), and elemental analysis. In the FT-IR spectra the band corresponding to the symmetric stretching vibration C=C st appears at 1644 cm^{-1} while the signal corresponding to the C-C vibrations of the aza-aromatic rings is located at 1475 cm^{-1}. At 1253 cm^{-1} can be observed the band corresponding to the symmetric tension vibration C=N st. The ^{13}C CP-MAS NMR spectrum is also in agreement with the formation of the Aza-CMP material as it shows three signals corresponding to the three different carbon atoms in the polymer. The signal at 141 ppm corresponds to the carbon atoms of the phenyl edges connected to aza units, the signal at 129 ppm can be assigned to the carbon atoms of the triphenylene cores on vertices, and the signal at 105 ppm is due to the carbon atoms of the phenyl edges.
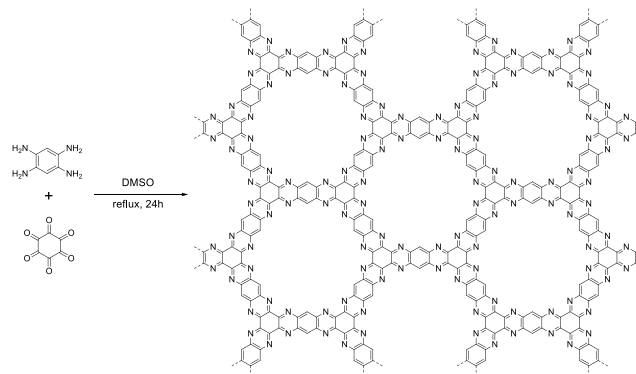

Figure 1. Formation reaction and structure of **Aza-CMP**.

Thermogravimetric analysis of **Aza-CMP** shows <10% weight loss at 150 °C assigned to the loss of volatiles (H_2O, DMF) trapped in the pores (figure S3). At 250 °C the material starts its chemical decomposition showing <20% weight loss at 450 °C indicating the good thermal stability of **Aza-CMP**. The presence of the trapped solvent at the pores can explain the discrepancies observed for the observed elementary analysis (C, 52.47 %; H, 3.84 %; N, 23.92 % *vs* theoretical values calculated for $C_{15}H_3N_6$: C, 67.42 %; H, 1.13 %; N, 31.45 %). In agreement to similar Aza-CMPs,[22] **Aza-CMP** is amorphous and do not show clear peaks in X-ray powder diffraction measurements (Figure S4). To investigate the porous structure of **Aza-CMP**, nitrogen sorption isotherms were measured at 77 K (Figure S5). **Aza-CMP** exhibits typical type I isotherms, which are characteristic of microporous materials. The Brunauer-Emmet-Teller (BET) surface area and pore vol-

ume of **Aza-CMP** were calculated to be 566 m^2/g and 0.29 cm^{3}g^{-1}, respectively.

Interestingly, pressed pellets of **Aza-CPM** shows an AC conductivity value of 3×10^{-5} Sm^{-1} that can contribute to its electrocatalytic performances. (Figure S6).

Figure S7 provides large area atomic force microscopy (AFM) images of diluted suspensions of **Aza-CMP** deposited by drop-casting on SiO$_2$ (SI for experimental details). The topographic images show large density of nanolayers with minimum heights of *ca.* 2 nm and over micron length lateral dimensions. This picture suggests a morphological description of the **Aza-CMP** material deposited on the electrodes.

The effective incorporation of the Co(II) into the **Aza-CMP@Co** was examined by XPS. The Co 2p spectra (figure S8) shows four peaks at 780.7, 782.5, 785.7 and 788,8 eV, which are in agreement with those observed in Co(II) complexes with nitrogen ligands.[31] Thus, the spectra indicates that the Co(II) is incorporated into the Aza-CMP forming complexes with the nitrogen atoms in the lattice.

Electrochemical behavior of Aza-CMP. Effect of the modification with Co. Prior to the ORR experiments, the behavior of **Aza-CMP** with and without cobalt modification was electrochemically characterized in 0.1 M NaOH. Figure 2 shows the voltammetric profiles of the glassy carbon supporting electrode alone, and with the deposit of the **Aza-CMP** unmodified and modified with Co(II). As can be seen, after the deposition of the **Aza-CMP**, the apparent double layer of the electrode slightly increases and a new pair of very small peaks appear at 0.16 V. The apparent double layer in carbon materials is mainly related to the redox chemistry of the functionalities present in the carbon. The virtual invariance of the double layer indicates that the **Aza-CMP** material does not have any functional groups in the material capable of having a redox process, aside from those related to the peaks at 0.16 V, which assures the quality of the material. This latter peaks can be associated to the hydrogenation of the nitrogen atoms, as has been proposed for nitrogen-doped graphene[32] according to the following reaction:

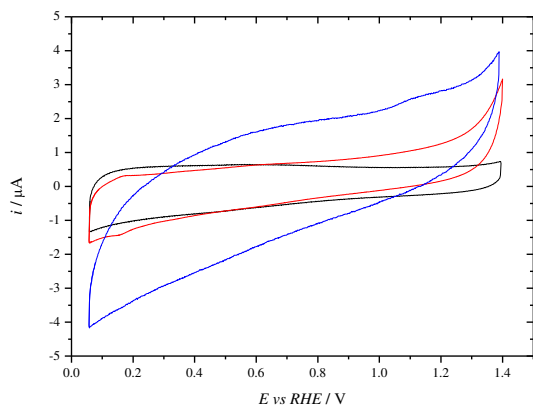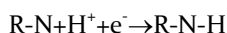$$R\text{-}N + H^+ + e^- \rightarrow R\text{-}N\text{-}H$$

Figure 2. Voltammetric profiles of the **Aza-CMP** (red line), **Aza-CMP@Co** (blue line) and modified glassy carbon (black line) electrodes in 0.1 M NaOH. Scan rate: 50 mV s^{-1}.

When the **Aza-CMP** material is modified with Co(II), the double layer increases, which clearly indicates that the cobalt has been clearly incorporated into the **Aza-CMP** materials (Figure 2). However, the peaks at 0.16 V disappear. It is expected that Co(II) is incorporated into the **Aza-CMP** by complexing to the nitrogen atoms. Thus, the complexation would prevent the hydrogenation reaction of the N atoms, leading to the disappearance of the peak. An additional proof that the effective incorporation of the Co(II) into the material can be obtained when the hydrogen evolution reaction is studied on those materials. Carbon is a very bad catalyst for this reaction, as can be seen in Figure 3. At an overpotential of *ca.* -0.9 V, the measured currents for the reaction are almost negligible. On the other hand, it is known that metallic Co has some activity for the reaction, and thus the incorporation of cobalt atoms into the **Aza-CMP** network leads to a significant diminution of the overpotential for this reaction, with a practical onset for the reaction of *ca.* -0.5 V. This fact corroborates the incorporation of the Co(II) into the **Aza-CMP** material.
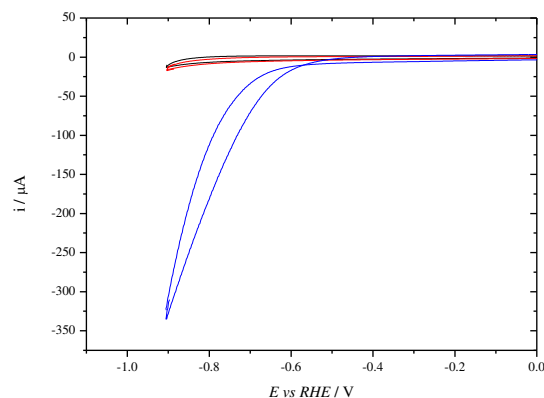
Figure 3. Voltammetric profiles of the **Aza-CMP** (red line), **Aza-CMP@Co** (blue line) and modified glassy carbon (black line) electrodes showing the hydrogen evolution reaction in 0.1 M NaOH. Scan rate: 50 mV s^{-1}.

Oxygen reduction reaction. Figure 4 shows the results for the ORR on the three electrodes. For the glassy carbon support, the activity is low. The onset for the glassy carbon electrode is *ca.* 0.55 V, and currents (in absolute values) show a slow increase as the potential is made more negative. This means that the reaction is mainly controlled by the kinetics of the process. Moreover, the process is not following the typical Butler-Volmer (B-V) kinetics. For B-V kinetics, a fast increase in the currents should be expected after the onset, as observed for metallic electrodes.[33] In this case, the increase is very gentle, and even a small plateau is observed around 0.4 V, suggesting that an inhibition process is taking place on the electrode as the potential is made more negative. This inhibition process is partially compensating the expected

increase for the B-V kinetics, giving rise to the observed moderate increase in currents. For an ideal electrocatalytst, the expected shape of the voltammetric profile would have a sigmoidal shape, reaching a maximum value, which is called limiting diffusion current. This current value is obtained when the electrode kinetics is very fast and the reaction rate is controlled by the diffusion of the reactants to the surface of the electrode. This diffusion limited current be easily calculated using the Levich equation:

$$i_{lim} = -0.62nAFD^{2/3}v^{-1/6}c_b\omega^{1/2}$$

where n is the number of electrons exchanged in the process, A is the geometrical area of the electrode, D is the diffusion coefficient, v, the kinematic viscosity, c_b, the bulk concentration of oxygen and ω, the rotation rate. Using the reported values D and c_b for oxygen and v, [34] and the geometrical area of the electrode (0.164 cm²), a current value of 0.450 mA is obtained when hydrogen peroxide is formed (n=2) or 0,900 mA for water (n=4). These values are equivalent to a current density values per geometrical area of 2.74 mA cm⁻² and 5.49 mA cm⁻², respectively.
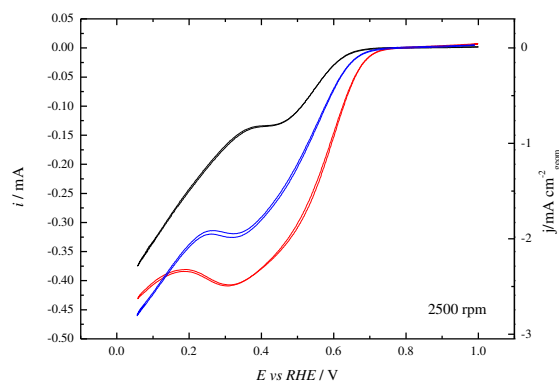

Figure 4. ORR reduction currents in a RDE for the **Aza-CMP** (red line), **Aza-CMP@Co** (blue line) and modified glassy carbon (black line) electrodes in O₂ saturated 0.1 M NaOH solution at 2500 rpm. Scan rate: 50 mV s⁻¹.

When the **Aza-CMP** was deposited on the glassy carbon, a significant increase in the electrocatalysis of the reaction is observed. The onset for the reaction is *ca.* 0.65 V and the increase in the current as the potential is made more negative is steeper than that observed in the GC. This fact clearly indicates that the **Aza-CMP** has higher activity for the ORR than the GC electrode. Moreover, around 0.4 V, the current reaches a quasi-steady state value, which is very close to the limiting current value for hydrogen peroxide formation. This would suggest that hydrogen peroxide is the main product of the reaction. As aforementioned, for this pH value, hydrogen peroxide is in the form of HOO⁻, (pka=11.65). On the other hand, the modification of the **Aza-CMP** with Co does not produces the expected behavior. Metallic modification of the carbon materials are normally linked to higher activity.[35] However, in this case, the onset is displaced to slightly

lower potential values and the currents are smaller than those recorded for the unmodified **Aza-CMP**.

In order to determine the final product in the reduction of oxygen, that is, whether hydrogen peroxide or water is obtained as final product, RRDE experiments were carried out. As aforementioned, the Pt ring is set at 1.1 V, so that the hydrogen peroxide can be detected. Figure 5 shows the currents measured in the ring (top panels) and disk (bottom panels) for the ORR. As can be seen, the shape of the current *vs.* potential for the ring and disk is symmetrical, which indicates that the ratio hydrogen peroxide/water production is almost independent of the electrode potential.
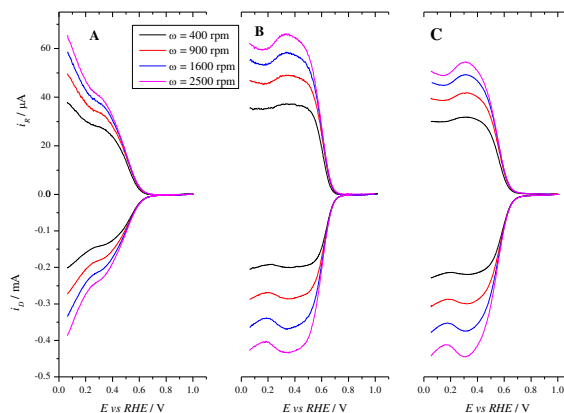

Figure 5. RRDE experiments for the ORR on the modified glassy carbon(A), **Aza-CMP** (B) and **Aza-CMP@Co** (C) electrodes in O₂ saturated 0.1 M NaOH solution at different rotation rates. Scan rate: 50 mV s⁻¹.

The quantitative analysis of the hydrogen peroxide production can be performed by analyzing the currents measured in the ring and disk electrodes. The total number of electrodes exchanged in the reduction process, n, can be calculated as follows:

$$n = 4\frac{I_D}{I_D + \frac{I_R}{N}}$$

where N is the collection efficiency of the ring (0.218 for the present geometrical arrangement), and I_D and I_R the measured currents for the disk and ring electrodes, respectively. Figure 6 shows the values on n calculated for the threes electrodes. As expected, the number of electrons is nearly independent of the potential. Moreover, the number is always close to two, revealing that the major product is always hydrogen peroxide. This number increases slightly when the **Aza-CMP** is modified with Co(II), indicating that the presence of Co catalyzes slightly the reduction of hydrogen peroxide to water. Therefore, **Aza-CMP** is an excellent electrocatalyst for the oxygen reduction to hydrogen peroxide. It must be highlighted that the equilibrium potential for this reaction is 0.68 V, and the onset potential obtained in the present conditions for the reaction is *ca.* 0.65 V, that is, the overpotential for effective currents in the reduction process of oxy-

gen to water peroxide is below 100 mV. Additionally, the current efficiency for hydrogen peroxide formation and selectivity of the reaction can be calculated using the ring and disk currents. As can be seen in Figure 7, the current efficiencies for the Aza-CMP is around 70% whereas the selectivity is above 80%, indicating the excellent performance of the catalyst.
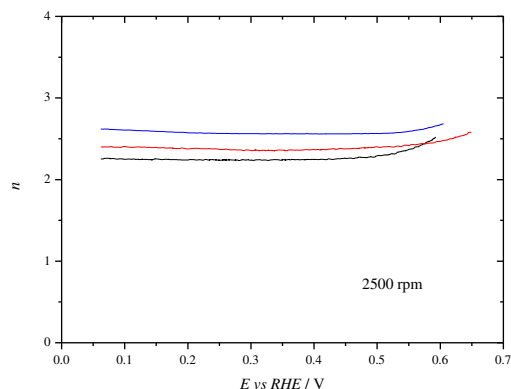

Figure 6. Dependence of the number of electrons transferred in the ORR reaction on the **Aza-CMP** (red line) and **Aza-CMP@Co** (blue line) modified glassy carbon (black line) electrodes in O_2 saturated 0.1 M NaOH solution.
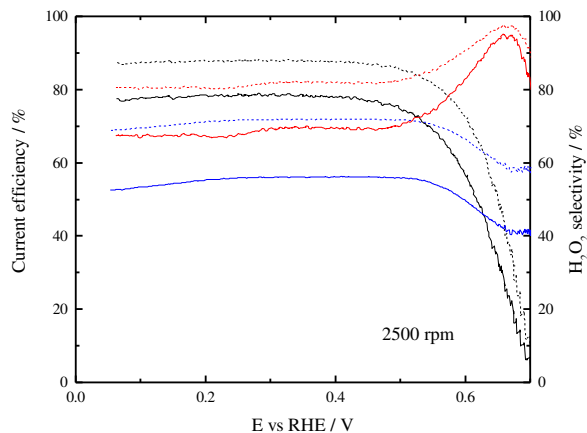

Figure 7. Current efficiency (full lines) and hydrogen peroxide selectivity for the ORR reaction on the **Aza-CMP** (red line) and **Aza-CMP@Co** (blue line) modified glassy carbon (black line) electrodes in O_2 saturated 0.1 M NaOH solution.

In order to determining the Tafel slope of the process, which provides some insight into the reduction mechanism, kinetic currents in absence of diffusion effects were calculated using the Koutecky-Levich analysis plots using the following equation:

$$\frac{1}{I} = \frac{1}{I_{kin}} + \frac{1}{B\omega^{1/2}}$$

where I_{kin} is the kinetic current, and B is the proportionality factor between the diffusion limiting current and $\omega^{1/2}$. Figure 7 shows the Tafel plots for **Aza-CMP** and **Aza-CMP@Co**. In both cases, Tafel slopes values are *ca.* 110 mV, which is normally associated with a mechanism in which the rate-determining step is the first electron transfer, that is, the formation of an adsorbed superoxide species according to the following reaction:

$$* + O_2 + e^- \rightarrow *\text{-}O_2^- \qquad (1)$$
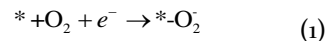
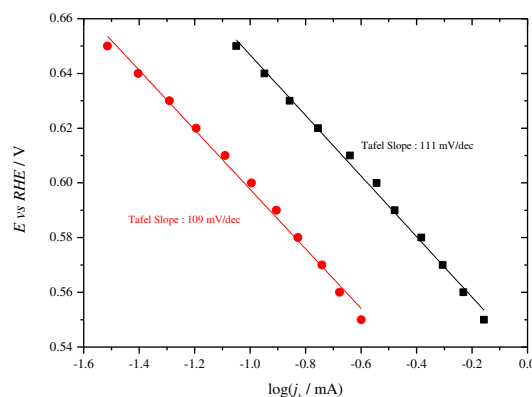where * denotes the active site on the material where the adsorption of O_2 takes place.

Figure 8. Tafel plots for the ORR obtained from the kinetics currents for the **Aza-CMP** (black line) and **Aza-CMP@Co** (red line).

DFT calculations on the reaction mechanism. The experimental results presented here show that the **Aza-CMP** material has excellent properties for the reduction of oxygen to hydrogen peroxide, being almost inactive for the reduction of hydrogen peroxide to water. Moreover, the kinetic analysis suggests that the rate determining step would be the adsorption process to yield a superoxide. For a better understanding of the electrocatalysis of the reaction and to determine the active site on the **Aza-CMP** material, DFT calculations have been carried out. In a previous work,[20] it was emphasized that, to activate oxygen on graphitic materials by means of monodentate chemisorption on carbon, two specific conditions would have to be fulfilled: a sufficiently destabilized carbon atom would have to be accessible and additional available charge would have to be provided. Changing from sp^2 hybridization state to sp^3, the destabilized carbon atom would bond to oxygen; meanwhile the available charge would be localized on the adsorbed oxygen, stabilized by the solvation effect. Therefore, the chemisorbed oxygen species would have superoxide characteristics, which has been identified as the first intermediate in the reaction. Additionally, in a recent previous work,[21] it has been pointed out that hydrogenated pyridinic nitrogen in graphitic materials would destabilize their adjacent carbon atoms, and that the charge involved in such a hydrogenation would remain segregated, becoming available for reduction processes. As can be observed in Figure 8,

which shows the periodic model of the **Aza-CMP** material used in our DFT calculations, the material presents several carbon atoms neighboring to pyridinic nitrogen that, if were hydrogenated, could promote the molecular oxygen activation. Therefore, prior to explore adsorption properties, the relevant hydrogenation state of the nitrogen atoms to consider should be determined.

Nitrogen atoms can be hydrogenated through the reaction

R-N + H$^+$ + e$^-$ → R-N-H
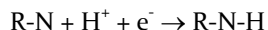
The standard redox potential of this process can be calculated using the approach introduced by Anderson and col.[19, 35] which uses the strength of the N-H bond and the standard redox potential for the reaction H$^+$(aq)+e = H(aq). In the initial lattice (Figure 8A), the position of all the nitrogen atoms is equivalent, but as the hydrogenation process on a first nitrogen atom takes place, the symmetry and equivalence of the nitrogen atoms is lost and differences in the energy of hydrogenation for the rest of nitrogen atoms appear. Figure 8B shows the order of hydrogenation process of the different nitrogen atoms and the energy of the N-H bond. The N-H bond energy of the nitrogen atom labeled as **1** is 3.39 eV, which corresponds to standard potential of 1.29 V, that is, a potential which is positive to the onset of the ORR. Moreover, the hydrogenation of this first nitrogen atom favors the hydrogenation of the opposite nitrogen one in the same ring, since now the bond energy is 3.6 eV.
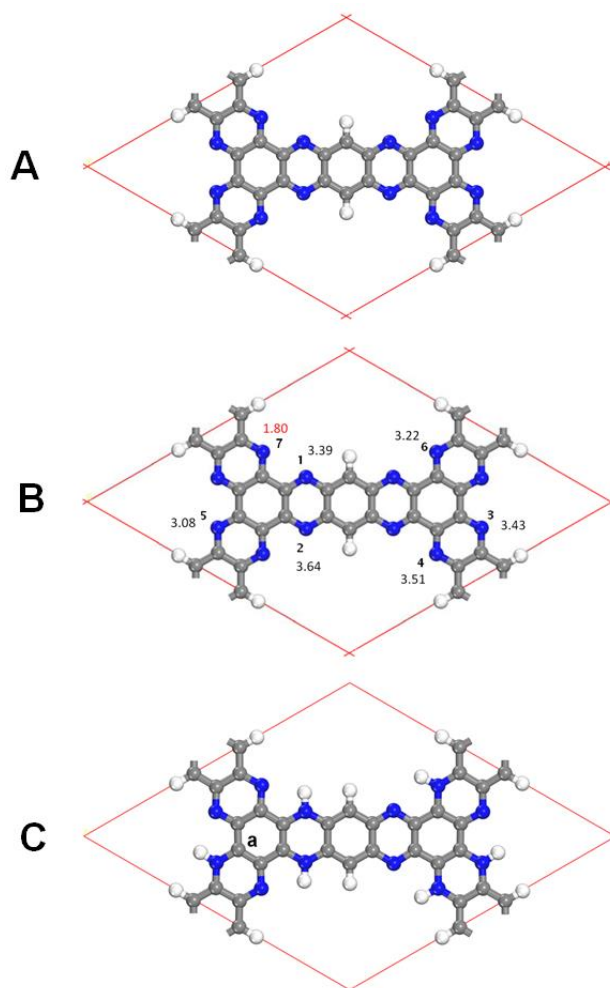

Figure 8. Periodic models of **Aza-CMP**. (A) Lattice (a broader supercell is also displayed in Figure S9). (B) Hydrogenation order of the pyridinic nitrogen atoms calculated by DFT and energies in eV of the process. (C) Relevant hydrogenation state (hexa-hydrogenated) and carbon atom tested as active site (labelled as **a**).

Then, it can be considered that both atoms hydrogenate simultaneously at a potential of *ca*. 1.3 V. The next atoms to be hydrogenated are those in the farthest ring in the lattice, those labelled as **3** and **4**, almost at the same potential. From that point, the hydrogenation process gets complicated due to the presence of steric problems. For instance, the hydrogenation of nitrogen atom labelled as **7** has steric repulsion due to the presence of a hydrogen atom in nitrogen atom **1**. Thus, the only nitrogen atoms in the cell for which there are no steric problems in the lattice are those labelled as **5** and **6**, which are hydrogenated at *ca.* 1.0-1.1 V. Finally, the N-H bond energy for carbon **7** is *ca.* 1.8 eV, which corresponds to a redox potential of *ca.* -0.3 V. All of these results clearly indicate that all the nitrogen atoms labelled from **1** to **6** would be hydrogenated at the onset of the ORR in a potential range between 1.1 and 1.4 V and no changes in the hydrogenation state of the material would occur during the ORR. In this sense, it should be noted that an oxidation current is measured

above 1.1 V in the voltammogram of Figure 2, which can correspond to the dehydrogenation process.
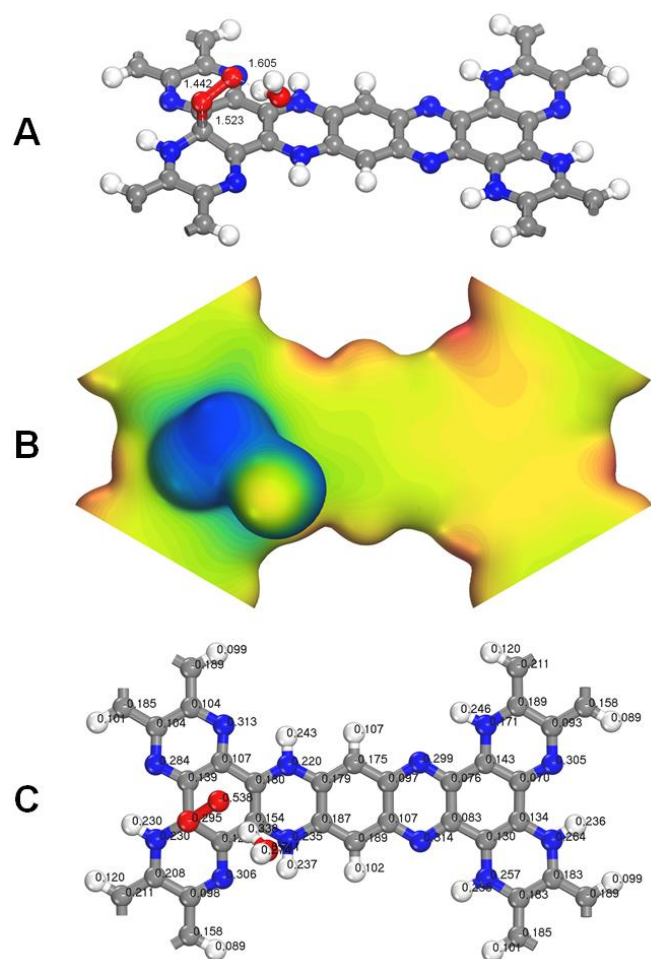

Figure 9. Monodentate chemisorbed state of molecular oxygen on the carbon atom labelled as **a** in Figure 8C. An explicit water molecule in addition to a continuum model was used as solvation effect treatment. (A) Adsorbent-adsorbate-solvent geometry [Å]. (B) Electrostatic potential [Ha/e⁻] mapped on the electron isodensity surface ρ = 0.01 e/Å³. (C) Mulliken partial charges [e⁻].

Once the relevant hydrogenation state of the **Aza-CMP** material has been determined (Figure 8C), the activity towards the ORR of the material and the active site can be investigated. To this end, the adsorption of O_2 to form a superoxide species, which is considered both the first step and also the limiting step of the whole of the process, is studied as in previous reports.[20-21] When the carbon atom labelled **a** in Figure 8C is tested for activation, under neutral charge conditions, the monodentate chemisorbed state of molecular oxygen displayed in Figure 9 is found, which is qualitatively similar to the ones previously found on others nitrogen-doped graphitic materials.[20-21] From Figure 9B can be appreciated that charge is contributed from the hydrogenated pyridinic nitrogen atoms to the adsorbed oxygen enabling the chemisorbed state. The partial charges of Mulliken displayed in Figure 9C assign *ca.* 0.83 e⁻ to the chemisorbed species, indicating clearly that it has superoxide characteristics. Moreover, in Figure

9A, the presence of an abnormally short hydrogen bond between the adsorbed oxygen and the explicit water molecule can be identified, evidencing the relevance of the stabilizing role played by the solvation effect. However, when the energetics of the process displayed in Figure 10 is considered, it can be observed that, despite de fact that the found chemisorbed state is favorable by 0.52 eV, it is only stable by *ca.* 0.11 eV when compared to the physisorbed state. The reason for so small stability would be that the carbon atom involved in the chemisorbed state would not be sufficiently destabilized. This observation would be completely consistent with previous results,[20] where it is found that hydrogenated pyridinic-nitrogen dopants in graphitic materials destabilize their adjacent carbon atoms mainly at armchair edges, giving rise to less effective destabilization at zig-zag edges. Moreover, the consequence of this observation would be key for hydrogen peroxide production purposes. Being a clearly favorable step, molecular oxygen could be activated. However, supporting only slightly stable chemisorbed states, the scission of the O-O would be hindered, originating the selectivity towards the hydrogen peroxide production. Other carbon atoms were also explored for activation, though no additional insights were found.
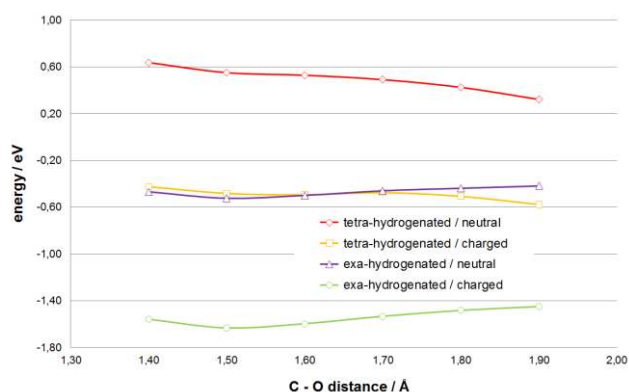

Figure 10. Total energies, referred to their respective references (adsorbent energy plus that corresponding to the adsorbate complex in the bulk), for an oxygen molecule located on top of the carbon atom a, for the different configurations estimated at different constrained distances between the carbon atom and the nearest oxygen atom of the molecule. Five explicit water molecules in addition to a continuum model were used as solvation effect treatment. A typical configuration of the formed explicit water solvation shell can be observed in Figure S10.

Given that, as the potential is made more negative, the charge of the electrode becomes more negative, the effect of the electrode potential can be examined by adding negative charge to the model. Moreover, such a kind of result can be used to explain the differences between the reactivity in acid and alkaline solutions. As the pH increases, the potential in the SHE scale at which the ORR shifts towards more negative potential values, and therefore, the surface charge of the electrode becomes more negative. For this case (Figure 8C), when a negative charge is added to the model, the adsorption energy for the oxygen species rises to 1.63 eV, meanwhile the stabil-

ity in comparison with the physisorbed state rises to 0.18 eV, indicating that as the potential is made more negative (or the pH increases) the formation of the adsorbed superoxide species is more favorable. This effect explains the increased activity of the material as the pH increases, since the observed activity in acidic solutions is very low.

In brief, as it has been introduced, the formation of the chemisorbed superoxide poses two conditions: a carbon that is able to shift from a sp^2 to sp^3 hybridization and charge supplied by the material. In this case, the presence of a hydrogenated nitrogen atom neighboring the studied carbon atom facilitates the hybridization state switching, whereas the charge is supplied from other hydrogenated nitrogen atoms. Therefore, the hydrogenation of the nitrogen atoms is a key element in this mechanism. When only four hydrogenated nitrogen atoms are considered, the adsorbed state becomes unstable, preventing the reaction, as observed in Figure 10. The investigated chemisorbed state becomes more stable when the charge becomes negative.

In comparison with other investigated carbon materials,[13] the activity of the **Aza-CMP** material used as electrode for the ORR is smaller, though its selectivity towards the production of hydrogen peroxide is higher. Both observations can be explained by the lower stability of the adsorbed superoxide state on the investigated material in comparison with those present in other graphitic materials.[20-21] An activating step less favorable implicates a smaller activity an adsorbed superoxide state presenting lower stability implicates that the adsorbate can be more easily desorbed upon protonation to the solution to yield HOO^- in alkaline media.

CONCLUSION

An electrochemical cell of hydrogen peroxide production requires of a catalyst for the oxygen reduction reaction optimally selective towards the target species. Moreover, the optimization of a catalyst requires of the control not only of the composition but also of the microstructure. The assembling of materials from molecular building blocks provides an excellent framework to achieve such a kind of control. Here, by using a polycondensation reaction between 1,2,4,5-benzenetetramine tetrahydrochloride and triquinoyl octahydrate, an aza-fused π-conjugated microporous polymer has been synthesized. The material shows excellent electrocatalytic properties for hydrogen peroxide formation at low overpotentials. The well-defined molecular structure of the polymer has allowed the use of DFT calculations to study the reduction mechanism and identifying the key elements that activate the material for the reaction. Thus, it has been shown that the hydrogenation of the nitrogen atoms is a key element in the activation of the neighboring carbon atom to adsorb oxygen.

ASSOCIATED CONTENT

Supporting Information. Additional experimental characterization data of the materials and computational details are provided as Supporting Information. This material is available free of charge via the Internet at http://pubs.acs.org.

AUTHOR INFORMATION

Corresponding Author

* enrique.herrero@ua.es, felix.zamora@uam.es

Author Contributions

The manuscript was written through contributions of all authors. All authors have given approval to the final version of the manuscript.

REFERENCES

1. Hernández, J.; Herrero, E.; Solla-Gullón, J.; Vidal-Iglesias, F. J.; Feliu, J. M.; Aldaz, A., Shape-Dependent Electrocatalysis: Oxygen Reduction on Gold Nanoparticles. In *Electrocatalysis: Proceedings of the International Symposium*, Brisard, G. M.; Adzic, R. R.; Birss, V.; Wieckowski, A., Eds. The Electrochemical Society Inc.: 2006; Vol. PV 2005-11, pp 200-212.

2. Mo, Y. B.; Scherson, D. A., Platinum-Based Electrocatalysts for Generation of Hydrogen Peroxide in Aqueous Acidic Electrolytes - Rotating Ring-Disk Studies. *J. Electrochem. Soc.* **2003,** *150*, E39-E46.

3. Siahrostami, S.; Verdaguer-Casadevall, A.; Karamad, M.; Deiana, D.; Malacrida, P.; Wickman, B.; Escudero-Escribano, M.; Paoli, E. A.; Frydendal, R.; Hansen, T. W.; Chorkendorff, I.; Stephens, I. E. L.; Rossmeisl, J., Enabling Direct H2O2 Production through Rational Electrocatalyst Design. *Nat. Mater.* **2013,** *12*, 1137-1143.

4. Verdaguer-Casadevall, A.; Deiana, D.; Karamad, M.; Siahrostami, S.; Malacrida, P.; Hansen, T. W.; Rossmeisl, J.; Chorkendorff, I.; Stephens, I. E. L., Trends in the Electrochemical Synthesis of H2O2: Enhancing Activity and Selectivity by Electrocatalytic Site Engineering. *Nano Lett.* **2014,** *14*, 1603-1608.

5. Maldonado, S.; Stevenson, K. J., Direct Preparation of Carbon Nanofiber Electrodes Via Pyrolysis of Iron(Ii) Phthalocyanine: Electrocatalytic Aspects for Oxygen Reduction. *J. Phys. Chem. B* **2004,** *108*, 11375-11383.

6. Ozaki, J.-i.; Tanifuji, S.-i.; Kimura, N.; Furuichi, A.; Oya, A., Enhancement of Oxygen Reduction Activity by Carbonization of Furan Resin in the Presence of Phthalocyanines. *Carbon* **2006,** *44*, 1324-1326.

7. Ozaki, J.-i.; Kimura, N.; Anahara, T.; Oya, A., Preparation and Oxygen Reduction Activity of Bn-Doped Carbons. *Carbon* **2007,** *45*, 1847-1853.

8. Gong, K.; Du, F.; Xia, Z.; Durstock, M.; Dai, L., Nitrogen-Doped Carbon Nanotube Arrays with High Electrocatalytic Activity for Oxygen Reduction. *Science* **2009,** *323*, 760-764.

9. Lefevre, M.; Proietti, E.; Jaouen, F.; Dodelet, J. P., Iron-Based Catalysts with Improved Oxygen Reduction Activity in Polymer Electrolyte Fuel Cells. *Science* **2009,** *324*, 71-74.

10. Wu, G.; More, K. L.; Johnston, C. M.; Zelenay, P., High-Performance Electrocatalysts for Oxygen Reduction Derived from Polyaniline, Iron, and Cobalt. *Science* **2011,** *332*, 443-447.

11. Jaouen, F.; Proietti, E.; Lefevre, M.; Chenitz, R.; Dodelet, J.-P.; Wu, G.; Chung, H. T.; Johnston, C. M.; Zelenay, P., Recent Advances in Non-Precious Metal Catalysis for Oxygen-Reduction Reaction in Polymer Electrolyte Fuel Cells. *Energy Environ. Sci.* **2011,** *4*, 114-130.

12. Lyth, S. M.; Nabae, Y.; Moriya, S.; Kuroki, S.; Kakimoto, M.-a.; Ozaki, J.-i.; Miyata, S., Carbon Nitride as a Nonprecious Catalyst for Electrochemical Oxygen Reduction. *J. Phys. Chem. c* **2009,** *113,* 20148-20151.
13. Zheng, Y.; Jiao, Y.; Chen, J.; Liu, J.; Liang, J.; Du, A.; Zhang, W.; Zhu, Z.; Smith, S. C.; Jaroniec, M.; Lu, G. Q.; Qiao, S. Z., Nanoporous Graphitic-C3n4@Carbon Metal-Free Electrocatalysts for Highly Efficient Oxygen Reduction. *J. Am. Chem. Soc.* **2011,** *133,* 20116-20119.
14. Xiang, Z.; Xue, Y.; Cao, D.; Huang, L.; Chen, J.-F.; Dai, L., Highly Efficient Electrocatalysts for Oxygen Reduction Based on 2d Covalent Organic Polymers Complexed with Non-Precious Metals. *Angew. Chem. Int. Ed.* **2014,** *53,* 2433-2437.
15. Ma, W.; Yu, P.; Ohsaka, T.; Mao, L., An Efficient Electrocatalyst for Oxygen Reduction Reaction Derived from a Co-Porphyrin-Based Covalent Organic Framework. *Electrochem. Commun.* **2015,** *52,* 53-57.
16. Wu, J.; Zhang, D.; Niwa, H.; Harada, Y.; Oshima, M.; Ofuchi, H.; Nabae, Y.; Okajima, T.; Ohsaka, T., Enhancement in Kinetics of the Oxygen Reduction Reaction on a Nitrogen-Doped Carbon Catalyst by Introduction of Iron Via Electrochemical Methods. *Langmuir* **2015,** *31,* 5529-5536.
17. Liu, X.; Li, L.; Zhou, W.; Zhou, Y.; Niu, W.; Chen, S., Inside Cover: High-Performance Electrocatalysts for Oxygen Reduction Based on Nitrogen-Doped Porous Carbon from Hydrothermal Treatment of Glucose and Dicyandiamide (Chemelectrochem 6/2015). *ChemElectroChem* **2015,** *2,* 770-770.
18. Ikeda, T.; Boero, M.; Huang, S.-F.; Terakura, K.; Oshima, M.; Ozaki, J.-i., Carbon Alloy Catalysts: Active Sites for Oxygen Reduction Reaction. *J. Phys. Chem. c* **2008,** *112,* 14706-14709.
19. Sidik, R. A.; Anderson, A. B.; Subramanian, N. P.; Kumaraguru, S. P.; Popov, B. N., O2 Reduction on Graphite and Nitrogen-Doped Graphite: Experiment and Theory. *J. Phys. Chem. B* **2006,** *110,* 1787-1793.
20. Ferre-Vilaplana, A.; Herrero, E., Charge Transfer, Bonding Conditioning and Solvation Effect in the Activation of the Oxygen Reduction Reaction on Unclustered Graphitic-Nitrogen-Doped Graphene. *Phys. Chem. Chem. Phys.* **2015,** *17,* 16238-16242.
21. Ferre-Vilaplana, A.; Herrero, E., Understanding the Chemisorption-Based Activation Mechanism of the Oxygen Reduction Reaction on Nitrogen-Doped Graphitic Materials. *Electrochim. Acta* **2016,** *204,* 245-254.
22. Kou, Y.; Xu, Y.; Guo, Z.; Jiang, D., Supercapacitive Energy Storage and Electric Power Supply Using an Aza-Fused Π-Conjugated Microporous Framework. *Angew. Chem. Int. Ed.* **2011,** *50,* 8753-8757.
23. Garsany, Y.; Baturina, O. A.; Swider-Lyons, K. E.; Kocha, S. S., Experimental Methods for Quantifying the Activity of Platinum Electrocatalysts for the Oxygen Reduction Reaction. *Anal. Chem.* **2010,** *82,* 6321-6328.
24. Garsany, Y.; Singer, I. L.; Swider-Lyons, K. E., Impact of Film Drying Procedures on Rde Characterization of Pt/Vc Electrocatalysts. *J. Electroanal. Chem.* **2011,** *662,* 396-406.
25. Perdew, J. P.; Burke, K.; Ernzerhof, M., Generalized Gradient Approximation Made Simple. *Phys. Rev. Lett.* **1996,** *77,* 3865-3868.
26. Delley, B., An All-Electron Numerical Method for Solving the Local Density Functional for Polyatomic Molecules. *J. Chem. Phys.* **1990,** *92,* 508-517.
27. Delley, B., From Molecules to Solids with the Dmol(3) Approach. *J. Chem. Phys.* **2000,** *113,* 7756-7764.
28. Neugebauer, J.; Scheffler, M., Adsorbate-Substrate and Adsorbate-Adsorbate Interactions of Na and K Adlayers on Al(111). *Phys. Rev. B* **1992,** *46,* 16067-16080.
29. Delley, B., The Conductor-Like Screening Model for Polymers and Surfaces. *Mol. Simul.* **2006,** *32,* 117-123.
30. Monkhorst, H. J.; Pack, J. D., Special Points for Brillouin-Zone Integrations. *Phys. Rev. B* **1976,** *13,* 5188-5192.
31. Ivanova, T.; Naumkin, A.; Sidorov, A.; Eremenko, I.; Kiskin, M., X-Ray Photoelectron Spectra and Electron Structure of Polynuclear Cobalt Complexes. *J. Electron Spectrosc. Relat. Phenom.* **2007,** *156–158,* 200-203.
32. Li, Q.; Noffke, B. W.; Wang, Y.; Menezes, B.; Peters, D. G.; Raghavachari, K.; Li, L.-s., Electrocatalytic Oxygen Activation by Carbanion Intermediates of Nitrogen-Doped Graphitic Carbon. *J. Am. Chem. Soc.* **2014,** *136,* 3358-3361.
33. Maciá, M. D.; Campina, J. M.; Herrero, E.; Feliu, J. M., On the Kinetics of Oxygen Reduction on Platinum Stepped Surfaces in Acidic Media. *J. Electroanal. Chem.* **2004,** *564,* 141-150.
34. Hsueh, K. L.; Gonzalez, E. R.; Srinivasan, S., Electrolyte Effects on Oxygen Reduction Kinetics at Platinum: A Rotating Ring-Disc Electrode Analysis. *Electrochim. Acta* **1983,** *28,* 691-697.
35. Kurak, K. A.; Anderson, A. B., Nitrogen-Treated Graphite and Oxygen Electroreduction on Pyridinic Edge Sites. *J. Phys. Chem. c* **2009,** *113,* 6730-6734.

SYNOPSIS TOC. In this work we show the excellent electrocatalitic performance for the hydrogen peroxide production of a robust aza-fused π-conjugated microporous framework. Its reaction mechanism has been rationalized using theoretical calculations.